

Estimating the Characterization of UMW by Correlate in online Sensor Signals with the Welding attributes



Ramesh Babu Yeluri

Assistant Professor,

Department of Mechanical Engineering,

Avanathi Institute of Engineering and Technology, Hyderabad -500078, India.

ABSTRACT:

The aim of this paper at present scenario about online process monitoring in ultrasonic welding of automotive lithium-ion batteries is essential for robust and reliable battery pack assembly. i.e UMW(Ultrasonic Metal Welding) This study provides a guideline for feature selection and advanced diagnostics to achieve a reliable online quality monitoring system in ultrasonic metal welding. analyses can be made with this information qualitative and quantitative, The effective quality monitoring algorithms have been developed to identify out of control parts by applying purely statistical classification methods. However, such methods do not provide the deep physical understanding of the manufacturing process that is necessary to provide diagnostic capability when the process is out of control. A deep understanding in these relationships will enable a significant reduction in production launch time and cost, improve process design for ultrasonic welding, and reduce operational downtime through advanced diagnostic methods. The purpose of this study is to determine the physical correlation between ultrasonic welding signal features and the ultrasonic weld-ing process conditions and ultimately joint performance. In this study, the fundamental physics behind the ultrasonic welding process is investigated using two process signals, weld power and horn displacement. Several online features are identified by examining those signals and their variations under abnormal process conditions. The joint quality is predicted by correlating such online features to weld attributes such as bond density and postweld thickness that directly impact the weld performance.

1 INTRODUCTION:

The welding process is used by many manufacture companies and due to this wide application many studies have been carried out in order to improve the quality and to reduce the cost of welded components. Part of the overheads is employed in final inspection, which begins with visual inspection, followed by destructive and non- destructive testing techniques. In addition to cost raise, final inspection is conducted when the part is finished only. When a defect occurs during welding, it can be reflected in the physical phenomena involved: magnetic field, electric field, temperature, sound pressure, radiation emission and others. Thus, if a sensor monitor one of these phenomena, it is possible to build a system to monitor the weld quality Ultrasonic metal welding is one of the processes used to join automotive lithium-ion batteries [1–3]. In ultrasonic metal weld-ing, a high frequency shear oscillation generated by a piezoelectric system, as described in Fig. 1, removes surface oxides or contamination by friction [4–6].

The continuous sliding action under pressure yields an increase in metal contact area, resulting in metallurgical adhesion [7–9] or diffusion [10,11] at the metal contact interfaces. These solid-state bonding characteristics are advantageous for joining dissimilar metals such as copper, alumi-num, and nickel, commonly used materials for battery tabs. In addition, the temperature of this process does not exceed the melting point of the metal workpiece, avoiding undesirable inter-metallic compounds and metallurgical defects that can result from most fusion welding processes [12]. Therefore, the ultrasonic welding process is well suited for battery tab joining. In a typical battery pack for hybrid and electric vehicles, sev-eral hundred battery cells are joined

together through tabs and For the automation and control of complex manufacturing systems, a great deal of progress came up in the last decade, with respect to precision and on-line documentation (bases for the quality control). With the advent of electrically driven mechanical manipulators and later the whole, relatively new, multidisciplinary mechatronic engineering, the need of information acquisition has increased. bus-bars to meet the desired power and energy capacity require-ments. The battery joints should possess reliable electrical con-nections as well as robust mechanical strength because failure of a single weld can result in degradation in performance, even fail-ure, of the entire battery pack. Therefore, quality monitoring is essential to ensure quality on every battery joint. As a quality assurance method, online process monitoring is widely used in manufacturing to ensure joint quality and process stability [13,14]. Although monitoring algorithms can be developed by systematic feature selection from various online signals utilizing

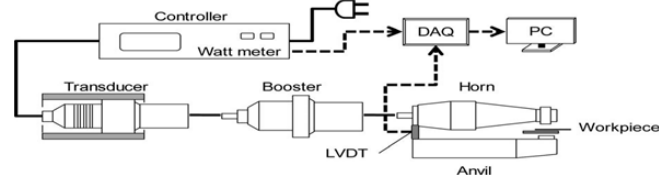


Fig. 1 Ultrasonic metal welding system and sensor signal acquisition

appropriate statistical methods without expert fundamental knowl-edge of the process [15], the selected features may not perform well when new abnormal process conditions are encountered. Thus, in order to develop a robust and reliable monitoring system, a fundamental understanding of sensor signals and their relation-ship to the welding process and eventually to weld quality should be established. A significant amount of research has been done on the relation-ship between sensor signals and weld quality for various welding technologies. For example, Ling et al. [16] predicted the quality of resistance spot welds by analyzing input voltage and current signals during the welding process. Li et al. [17] estimated resist-ance spot weld quality by correlating online signal features such as dynamic resistance with nugget size. Tseng and Chuang [18] showed the influence of maximum electrode displacement on the nugget diameter and thickness in predicting spot weld quality. Park and Kim [19] indicated that the plasma light intensity obtained by optical sensors could express the plasma/keyhole behavior, which directly impacts laser

weld quality. A compre-hensive review was performed by Sun et al. [20] on the usage of multiple sensors in real-time monitoring of laser weld quality and incorporation of sensor fusion with a neural network approach. In gas metal arc welding, the welding voltage and current signals were correlated to the weld quality using a statistical process con-trol method by Wu et al. [21]. Nevertheless, only limited research has been carried out on the sensor signals and their relationship to weld quality in ultrasonic metal welding. Or et al. [22] utilized a piezoelectric sensor to evaluate the weld quality during the ultra-sonic wire-bonding process, which was different from ultrasonic welding for sheet metals. They monitored the changes in resonant frequency or vibration amplitude caused by mechanical imp-dance change in the bonding zone.

Zhao et al. [23] developed a measurement system for monitoring transient temperature during the ultrasonic welding process using thin-film thermocouples fabricated on silicon substrates and inserted in a premachined slot in the weld tool. Their study showed that the heat flux and its rate change during the welding process provides good physical under-standing of ultrasonic bonding at the weld interface [24]. The methodology provided in their study showed some feasibility for process monitoring and control. However, no further examination was conducted on how the temperature would vary when abnor-mal situations occurred during the process. As a potential nondes-ruptive testing for ultrasonic welding, an experimental study on identifying effective welded area using a new shearography sys-tem has been carried out by Jia et al. [25]. In a previous study on ultrasonic welding of battery tabs [3], several weld attributes, such as bond density and postweld thickness, were identified from optical micrographs and correlated to weld quality. According to this study, the performance of an ultrasonic metal weld, such as mechanical strength, can be indi-rectly linked to process parameters through such attributes.

How-ever, there are limitations of using weld attributes for process monitoring since they are only available through off-line postweld measurement. Therefore, this paper attempts to investigate the fundamental physics behind the weld formation in ultrasonic welding using sensor signals and relating them to weld attributes, which in turn determine the weld quality. The remainder of the paper is organized as follows. We start by summarizing the weld formation mechanism in ultrasonic metal welding.

Then, the experimental procedure and sensor signals are described and the signal variation under abnormal process conditions is analyzed. After that, the relationship between signal features and weld attributes is identified, which provides direct information of weld quality. Finally, conclusions are presented

2. WELD FORMATION MECHANISM IN ULTRASONIC METAL WELDING:

Ultrasonic metal welding is a solid-state welding process. The frictional work between the workpiece materials generated from high frequency vibration in combination with the normal force breaks and disperses surface films (oxides, contaminants, etc.), and increases the actual contact area at the weld interface. This leads to localized intimate contact between exposed metal surfaces to form metallurgical bonds, which are atomic bonds between the metal lattices [26]. These locally created bonds (i.e., micro-welds) increase in density over the region affected by the weld tip as a result of the rise in temperature caused by extensive plastic deformation. In addition to metallurgical adhesion, the continuous vibration and static force from the horn result in bonding lines that curl around the microwelds, and they play a role in mechanical interlocking. Thus, a weld in ultrasonic metal welding of similar materials, nickel plated copper in this paper, is formed mainly by metallurgical adhesion with partial aid of mechanical interlocking. Ultrasonic metal welding does not create any fusion zone where the temperature of the mating metals reaches the melting point.

Figure 2 shows the microstructure of weld sample cross sections of 1.1 mm nickel plated copper and 0.5 mm copper (C11000). After the nickel layer (less than 2 μm) is broken by the oscillating shear force, a unified grain structure between the two bare copper sheets is formed as shown in Fig. 2(a). The nickel layer is broken into pieces and it curls along the weld line producing interfacial hooks, as shown in Fig. 2(b). The interfacial hooks provide additional mechanical strength. In this paper, two key weld attributes which have a direct impact on the final weld performance, bond density, and postweld thickness, are measured and correlated with signal features. Bond density is the proportion of bonded region to the entire weld width while postweld thickness is the proportion of the indented thickness of the upper sheet to the original thickness.

These nondimensional parameters were defined in a previous study of joint quality characterization in ultrasonic metal welding by Lee et al. [3]. Figure 3 shows the effect of a key process variable, weld time, on

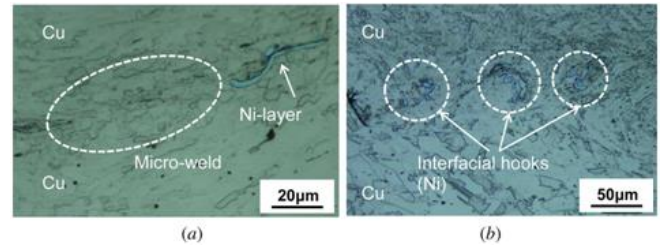


Fig. 2 Optical micrographs with two main bonding mechanisms for ultrasonic metal welds: (a) metallurgical bonding; and (b) mechanical interlocking [3]

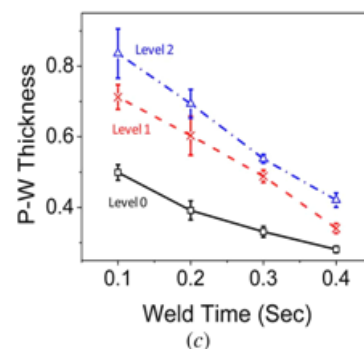
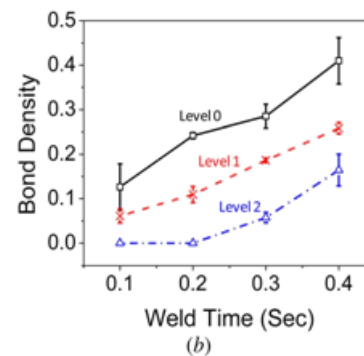
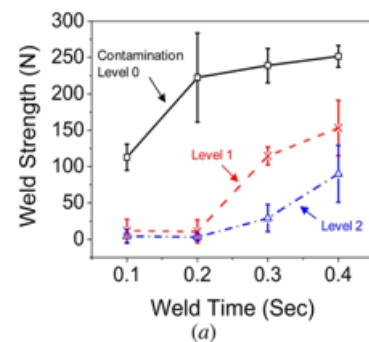


Fig. 3 Influence of weld time on (a) weld strength obtained from U-tensile test; (b) bond density; and (c) postweld thick-ness under different levels of contamination (level 0: cleaned with isopropyl alcohol, level 1: one drop of vanishing oil, level 2: two drops of vanishing oil)

joint performance, bond density and postweld thickness. As shown in Fig. 3(a), the weld strength increases dramatically in a short welding time. Then it shows a slow increase as welding time keeps increasing despite a steady increase of bond density as described in Fig. 3(b). This is caused by the decrease of postweld thickness over time as shown in Fig. 3(c), which may lead to excessive thinning of the material. Based on these results, the per-formance of an ultrasonic metal weld is in positive correlation with bond density while in negative correlation with postweld thickness. The welding process variation with contaminated surface in Fig. 3 is detailed as follows. An abnormal process condition was simulated by applying oil-based stamping fluid (Daphne vanishing oil) at the interface between the workpieces as surface contaminant. This has been reported in the assembly line of battery packs

Table 1 Factors and levels for experimental design

Welding time (s)	Surface contamination	Replicates	
		U-tensile test	Postweld measurement
0.1	Level 0	3	3
0.1	Level 1	3	3
0.1	Level 2	3	3
0.2	Level 0	3	3
0.2	Level 1	3	3
0.2	Level 2	3	3
0.3	Level 0	3	3
0.3	Level 1	3	3
0.3	Level 2	3	3
0.4	Level 0	12	3
0.4	Level 1	12	3
0.5	Level 2	12	3

as a possible source of contamination. The level of contamination was controlled by a transfer pipette providing 0.05 ml per drop. Three different levels of contamination were applied in this experiment:

level 0 (cleaned with isopropyl alcohol), level 1 (one drop of vanishing oil), and level 2 (two drops of vanishing oil). After the drops were applied and smeared over the surface evenly, the welding took place immediately to minimize the effect of oil evaporation on the result.

3 SENSOR SIGNALS FROM ULTRASONIC WELDING PROCESS:

In this section, the signals collected on an AmTech Ultraweld^{VR} L-20 high power welder are analyzed to describe the mechanism of weld formation during the ultrasonic welding process. The experimental procedure is described first. Then two sensor signals, power and displacement, are introduced, and their variations under surface contamination are examined.

3.1 Experiment. Prepared coupons of nickel plated copper sheets of dimensions 20 mm by 50 mm were welded for different welding times using the AmTech ultrasonic welder. The pressure and the vibration amplitude were fixed at 35 psi (241 kPa) and 40 μ m, respectively. The lap joint of two copper sheets of different thicknesses, 0.2 mm and 1.0 mm, was designed for simulating joints between battery tabs and bus-bars. Table 1 summarizes the factors, levels and corresponding replication for this experiment.

During the welding experiment, the power and displacement signals from the sensors built into the welder, as illustrated in Fig. 1, were collected and processed to analyze the relation between signal features and product or process quality. Three weld samples produced were then subjected to a U-tensile test for obtaining their mechanical properties. Another three weld samples were cross-sectioned, mounted, and polished using 0.03 μ m colloidal silica suspension followed by etching [3] in order to conduct further microscopy and weld attribute measurement. More replicates for 0.4 s weld time (twelve for tensile test; three for cross-sectioning) were made in order to have enough data to analyze the trend of sensor signals with fixed weld time.

3.2 Sensor Signals. Two sensor signals are analyzed: (1) the electric power required for maintaining the mechanical vibration of the weld tool (i.e., horn) and (2) the linear displacement of the horn in the clamping direction.

3.2.1 Power. The ultrasonic vibration is provided by a piezo-electric system and transmitted to a booster/horn

stack assembly with designated amplitude. To maintain this mechanical vibration at a constant level of amplitude, the amount of electrical power is controlled throughout the welding process depending upon the

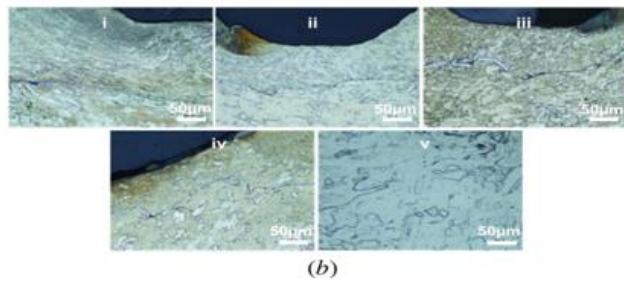
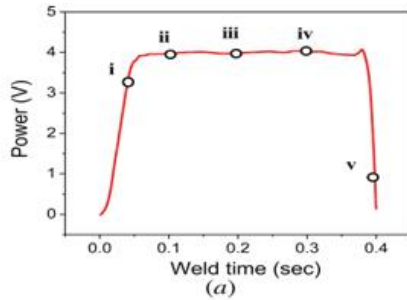


Fig. 4 Power signal variation over time: (a) power profile for a single welding cycle; and (b) continuous cross section images at the weld interface during welding cycle

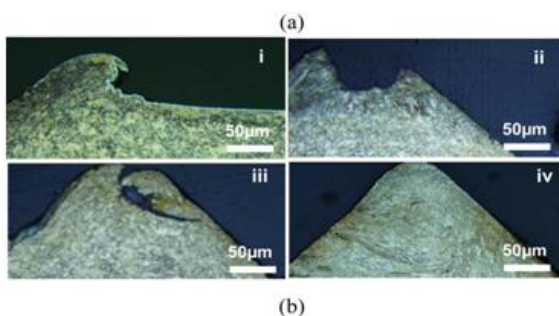
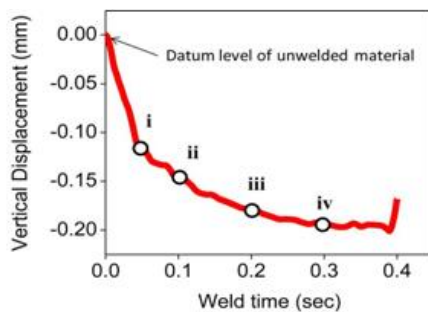


Fig. 5 LVDT signal: (a) horn displacement; (b) cross section images at the top of metal surface illustrating material filling behavior that corresponds to the displacements shown in (a)

mechanical loading conditions on the weld joint, which may vary during the process. The power can be defined as

$$Power = \frac{dS}{dt} \cdot \frac{1}{F} = \frac{1}{F} \cdot \frac{dS}{dt}$$

where F is the force exerted on the weld tip as a function of friction coefficient (μ) and clamping force (F_N), and $dS(t)/dt$ is the velocity profile of the weld tip function. Since the clamping force and the weld tip velocity are controlled at a constant value during the welding process, the power is only a function of friction coefficient. Therefore, the surface condition of the mating metal sheets directly impacts the power signal. Figure 4(a) shows the power required to initiate and maintain the vibration motion of the horn during the weld cycle and Fig. 4(b) the cross section images of the weld interface over welding time. As shown in Fig. 4(a), the power rapidly ramps up for the initial 0.1 s of welding time and stays at a constant level to maintain the vibration.

As ultrasonic energy is transmitted to the weld interface, the shear force generated from the high frequency lateral movement results in yielding of the material. Extensive plastic deformation or cold work is observed in the elongated grains along the bonding line as seen in the initial stage of weld process (Fig. 4(b)). As welding proceeds, severely deformed grains and the migration of high angle grain boundaries lead to the formation of a new grain structure (i.e., recrystallization) [27–29], and a continuous welding action with increased temperature results in growth of the recrystallized grains [3]. Those recrystallized grain structures are seen in most normal quality welds, which have already been described in many previous studies [3,27–29]. This is mainly due to the temperature rise at the weld interface with the aid of severe cold working of the material, which is caused from the dissipation of mechanical energy (i.e., vibration) by friction [30].

3.2.2 Displacement. A linear variable differential transformer (LVDT) was used to measure the horn displacement in the clamping direction. This signal data provides information on mechanical deformation, or material compaction, made by the knurl of the horn. The displacement profile as shown in Fig. 5(a) shows the trend typically seen in normal quality welds. In the initial stage of the welding process (<0.05 s), the material compaction of the material occurs at relatively high speed, but at a lower speed after that (>0.05 s).

Figure 5(b) describes a series of cross section images that impose a material filling phenomenon into the space between knurl peaks. Based on the findings from the previous study [3], the material compacts faster in this initial stage because material is being moved into the knurl through plastic displacement. Once the material fills the space, the compaction rate becomes slower. The fast initial compaction usually leads to a good quality weld since the full engagement of the tool and the material provides good sliding motions at the weld interface. The quality of ultra-sonic welds has a close relationship with the amount of material compaction. Thus, the linear displacement profile of the horn can be utilized as valuable data for process monitoring.

3.3 Signal Variation Under Process Disturbance. As discussed in Sec. 3.1, process disturbances during the ultrasonic welding process for battery tab joining were simulated by contaminating the workpiece surface with stamping fluid. The weld samples produced with three different levels of contamination—level 0, level 1, and level 2—are examined by microscopy. Figure 6(a) illustrates the typical trend of power signals for the three contamination levels during the welding process. Fifteen replicated signals were collected from the welding experiment, and all showed similar patterns. The power for welding of materials with clean surface shows a fast increase up to about 2300 W, followed by a steady power level until welding is over, whereas the power for both contaminated cases does not reach the same

power requirement as the clean surface case but only 70–75% of that (stage I in Fig. 6). Instead, the power decreases over a period of time (stage II) and gradually increases again (stage III) before settling as the end of the weld cycle is reached (stage IV). The lack of power ramp-up in stage I followed by a continuous reduction in stage II for contaminated surfaces mainly come from the low frictional resistance to the relative motion of metal sheets. So the welder does not require such high power to maintain the vibration with the designated amplitude. However, once the contaminants of the surface have been dispersed or removed, the welder regains its power in stage III as the friction resistance recovers back to the normal condition. The time duration for stage II depends on the amount of contamination at the interface as shown in Fig. 6(a).

Figure 6(b) shows the variation of the horn's absolute position during welding of copper sheets of different contamination levels. The same stage division as the power signal can be applied to this LVDT signal. At stage I, the horn abruptly decreases its position as the weld tool penetrates the metal surface even though the amount of material compaction with contaminated surface differs from one with clean surface. For surface contamination cases, the low power level in stage I causes less heat generation, which results in less softening of the material [3] and, therefore, less amount of material compaction. This penetration helps the weld tool fully engaged in the metal surface.

After the initial material compaction, the horn slows down its descent in stage II while very little descent is made for the contaminated surface case due to the decrease in power. Then, as the welder increases power again in stage III, the speed at which the horn is descending is regained whereas the horn slows down for clean surface case. Figure 7 is a series of microscopic images focused at the weld interface of a weld sample with clean surface. It shows that, as power increases and the horn lowers its altitude, the nickel layer is dispersed or broken apart by a shear force exerted on the interface. Microwelds are developed along the weld line, which becomes curled as welding proceeds. The micrographs shown in Fig. 8 indicate that the contaminants are trapped in the weld interface

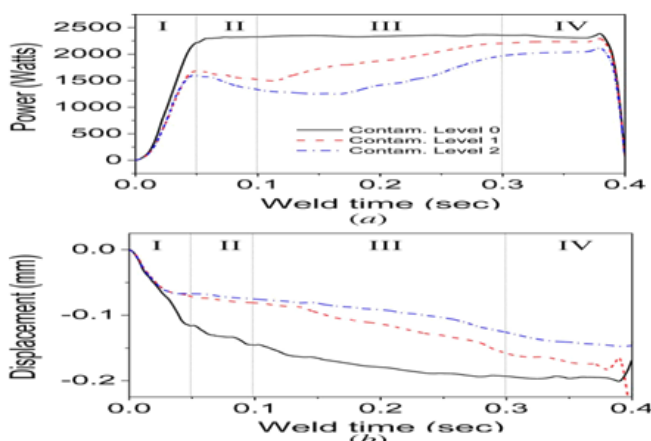


Fig. 6 Variation of (a) power signal and (b) displacement signal for different levels of surface contamination

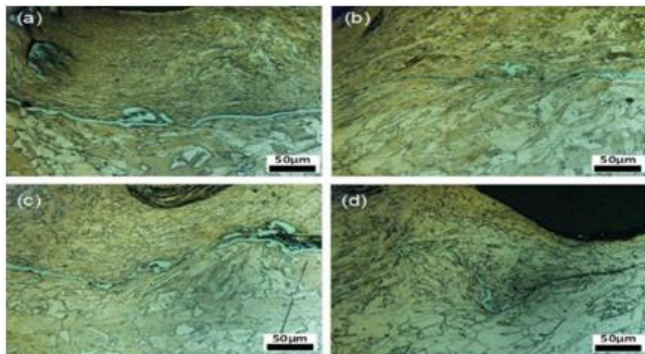


Fig. 7 Optical micrographs showing weld line formation with welding time of (a) 0.1 s, (b) 0.2 s, (c) 0.3 s, and (d) 0.4 s

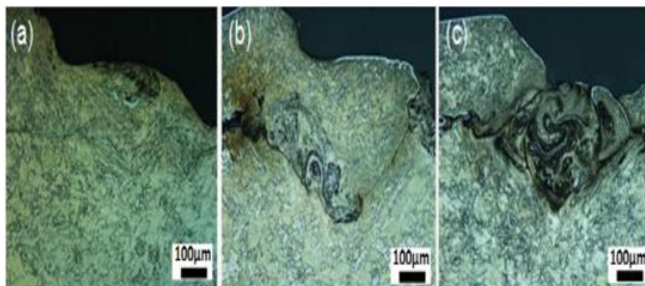


Fig. 8 Optical micrographs at the weld interface for three levels of surface contamination: (a) level 0 (clean); (b) level 1; and (c) level 2

and formed as a swirl, which makes the joint weaker. This is because the remaining oil layer in the early stages of the welding process hinders the adhesion of two metal surfaces and delays the weld development.

4 RELATIONSHIP BETWEEN WELD ATTRIBUTES AND SIGNAL FEATURES:

In this section, signal features are correlated to weld attributes to identify the relationship between sensor signals and product quality. First, several features in power and displacement profiles are introduced. Then, we present the feature variations during the welding process. Finally, the relationship between those features and weld attributes is presented.

4.1 Features From Online Signals.

Based on our understanding of the physics behind the signal variation under process disturbance as discussed in Sec. 3, the early stages of the welding process is crucial for sensing some abnormal process conditions. For example, the power required in this period changes depending on the level of surface contamination due to different friction conditions.

These different power levels lead to different amounts of material deformation, resulting in changes in horn displacement. Thus, the energy used and the amount of material compaction in this early stages are two important features in both power and displacement signals. For the simplicity of calculation, the energy is obtained from the beginning to the midpoint of the welding process. In the same manner, the amount of material compaction of the midpoint of the welding process is chosen as one feature of the displacement signal. Those two features are named E_{mid} and D_{mid} , respectively.

As discussed previously, an ultrasonic metal weld is formed through continuous rubbing action that yields an increase of bonded areas between clean metal surfaces. The curved weld line is found in typical weld samples with normal weld quality. The welding experiments performed in this paper show that the weld samples produced in 0.4 s welding time have the strongest joint performance owing to high bond density and reasonable amount of material compaction, as described in Fig. 3. Therefore, the normal quality weld requires a certain level of welding time or energy input. In that sense, total energy used and total amount of material compaction during the entire welding process are also important

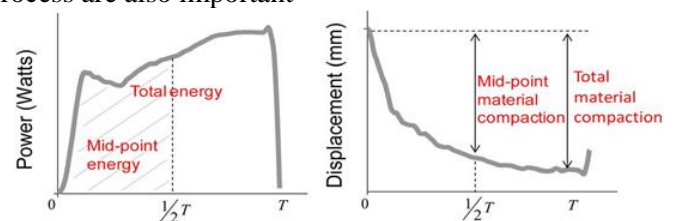


Fig. 9 Features in power and displacement signals

features in the power and displacement curves. They are named E_{total} and D_{total} , respectively. Figure 9 illustrates the main features measured in the power and displacement signals. Figure 10 shows the relationship between weld strength and each signal feature. As shown in Figs. 10(a) and 10(b), E_{total} and E_{mid} of the power signal for normal weld samples is clearly distinguished from those for problematic welds caused by surface contamination. D_{mid} , as a displacement signal feature, also shows the capability of separating normal and defective weld groups as described in Fig. 10(d) while D_{total} in Fig. 10(c) shows some capability to distinguish two weld groups but not as much as D_{mid} does. All these four features show a linear relationship with joint performance, indicating that the welds with higher strength possess higher E_{total} , E_{mid} , D_{total} or D_{mid} .

As indicated in all four plots, the amount of contaminants on the metal surface also affects the level of weld energy or the amount of material compaction. 4.2 Effect of Welding Parameters on Signal Features. For the signal features that have been identified, their relationships to a key process variable, welding time, are established in this subsection. E_{total} and D_{total} are plotted against welding time, as illustrated in Fig. 11, which shows that E_{total} and D_{total} increase linearly over time regardless of the level of surface contamination. As welding time increases, more ultrasonic energy is consumed for frictional heating, plastic deformation and bond formation at the interface. Consequently, more heat generated by increased weld energy yields softening of the material, resulting in larger amount of material compaction by the weld tool.

However, only a fraction of the energy is used for welding a surface contaminated workpiece. In the very early stages of the process (0.1 s), approximately 160 J is consumed for welding clean metals whereas only 60% of this energy is used for both contamination levels 1 and 2, as indicated in Fig. 11(a). As welding proceeds, the energy consumption for contamination level 1 and level 2 increases at different rates. At the very end of the welding process (0.4 s), approximately 82% energy of the clean surface case is used for level 1 contamination, and only 65% for level 2. This is because the larger amount of contaminants the workpiece possesses, the longer time is taken for removing the remaining contaminants by oscillating shears. D_{total} has a similar increasing trend with increasing weld time as E_{total} , as shown in Fig. 11(b), but the increasing rate depends on the level of contamination.

For example, the difference in post material compaction from 0.1 s to 0.4 s for level 0 is 0.19 mm whereas that for level 1 and level 2 is only 30% and 50% of level 0, respectively. In a similar manner to that for weld energy, material compaction for contaminated surface cases is slower than that for clean surface. 4.3 Relationship Between Weld Attributes and Signal Features. Weld attributes such as bond density and postweld thickness were defined as the physical criteria for weld quality in the previous study [3]. Correlating these attributes with signal features ensures good understanding of the weld formation during the

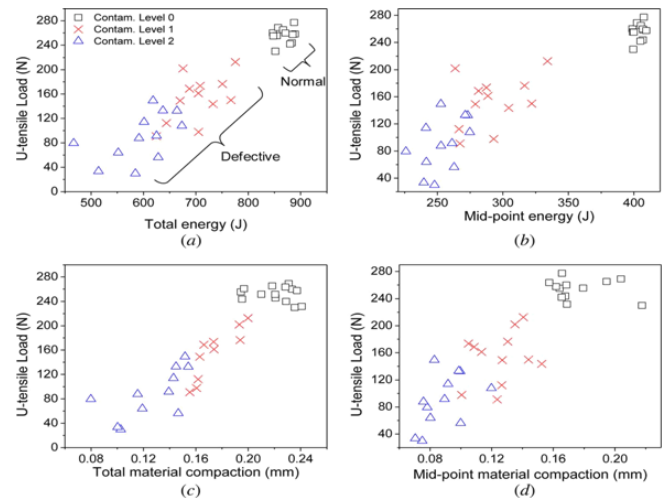


Fig. 10 Relationship between weld performance and signal features: (a) total energy (E_{total}); (b) midpoint energy (E_{mid}); (c) total material compaction (D_{total}); and (d) midpoint material compaction (D_{mid})

welding process so that the weld quality can be predicted by sensor signals. Figure 12 illustrates the relationship between weld attributes and the signal feature extracted from the power signal. As seen in Fig. 12(a), bond density and E_{total} are in a positive linear relation for both clean and surface contaminated case while a negative linear relation exists between postweld thickness and E_{total} as described in Fig. 12(b). Given the fact that normal quality welds that provide the highest joint performance in the preliminary U-tensile test (Fig. 3) have bond density around 40% and postweld thickness around 28%, the minimum required value for E_{total} can be set to around 800 J. Figures 12(c) and 12(d) describe the scatter plots of bond density and postweld thickness against another signal feature extracted from the power signal, E_{mid} .

As seen in the figure, E_{mid} of clean surface case is clearly distinguished from that of contaminated surface case. This ability of separating normal and problematic weld quality makes E_{mid} a valuable feature for contamination detection. The required energy level at the midpoint of welding process can be set to around 400 J in order to achieve 40% bond density and 28% postweld thickness. In addition to E_{total} and E_{mid} , D_{total} and D_{mid} also shows strong relationships to bond density or postweld thickness as illustrated in Fig. 13. Of those two features, D_{mid} , as shown in Figs. 13(c) and 13(d) has ability in discriminating between normal and defective weld groups that result from surface contamination. Process variation due to such abnormal condition mostly occurs during the early welding stages.

It should be noted that both E_{mid} and D_{mid}

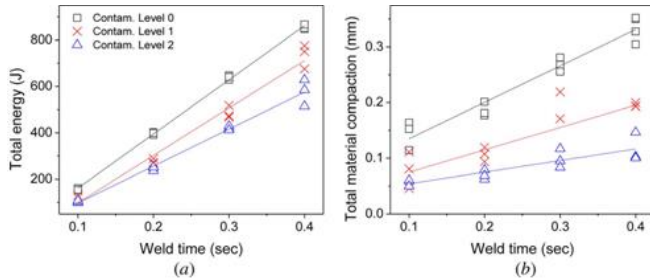


Fig. 11 Effect of welding time on: (a) total energy (E_{total}); and (b) total material compaction (D_{total})

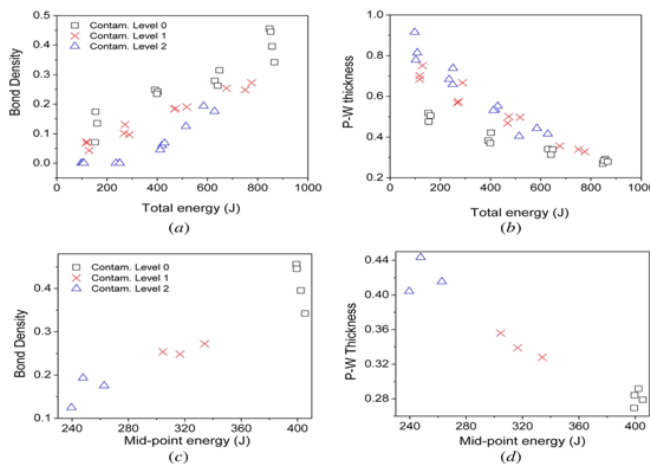


Fig. 12 Relationship between weld attributes and power signal features: (a) bond density versus total energy (E_{total}); (b) postweld thickness versus total energy (E_{total}); (c) bond density versus midpoint energy (E_{mid}); and (d) postweld thickness versus midpoint energy (E_{mid})

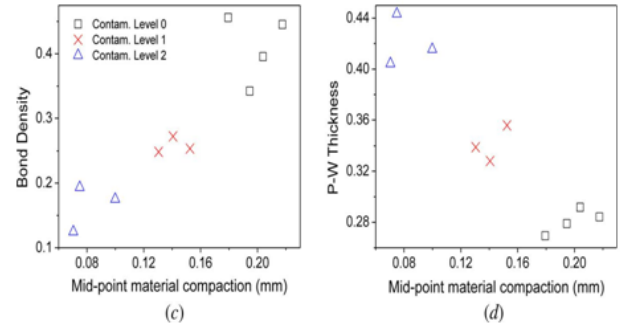
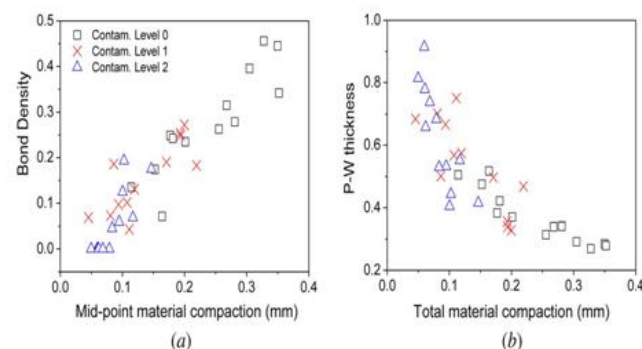


Fig. 14 Relationship between signal features: (a) midpoint material compaction (D_{mid}) versus midpoint energy (E_{mid}); (b) total material compaction (D_{total}) versus total energy (E_{total})

are the extracted features from the first half of the process. D_{total} of 0.3 mm or D_{mid} of 0.2 mm can be set as desired values for required postweld thickness of normal quality welds, as indicated in Figs. 13(a) and 13(b). By correlating online features to weld attributes, the physics behind the signal feature's change under process variation are understood: for example, one can learn how the feature variations are related to the change in geometric and mechanical attributes of an ultrasonic weld. Figure 14 shows the scatter plots of four online features, which enable the feasibility for online process monitoring to be ascertained. Figure 14(a) shows the direct relationship between two signal features, E_{mid} and D_{mid} , halfway through the welding process, while Fig. 14(b) shows the relationship between two features, E_{total} and D_{total} , collected after the process is over. Both E_{mid} and E_{total} clearly distinguish problematic weld group (contamination levels 1 and 2) from normal quality group (level 0). D_{mid} and D_{total} also show this discriminative capability, but not as clearly as E_{mid} and E_{total} in terms of the distance generated between two data groups (normal versus defective). E_{mid} and D_{mid} , can be used as in-line monitoring signatures since they capture the process variations in the early welding stages. A proper control action can then be taken, based on the characteristics shown in those signatures. On the other hand, E_{total} and D_{total} can be used as postweld monitoring signatures so that the product quality after welding can be determined.

5 CONCLUSIONS:

In this study, two online signals, weld power and horn displacement, are thoroughly examined to understand the physics behind the ultrasonic welding process. Several signal features are identified, based on the physical understanding of signal variations under

abnormal process conditions such as surface contamination. These signal features are then correlated to weld attributes measured from micrographs of cross-sectioned weld samples. By determining the relationship between those signal features and weld attributes, the joint quality can be predicted. This study will also provide a guideline for feature extraction/selection and setting criteria on selected features in process monitoring of ultrasonic metal welding. More specifically:

- (1) The power signal provides useful information on the change of mechanical resistance at the weld interface during the ultrasonic welding process whereas the displacement signal relates to the pattern of material deformation.
- (2) The power signal for the first half of the welding process provides critical information on the mechanical loading on the weld tool. A low level of weld power is experienced in the early welding stages under process disturbances such as low friction between surfaces due to residual stamping oil.
Similarly, the amount of material compaction at the mid-point of the process as measured by an LVDT also can be used to distinguish between normal and abnormal process conditions.
- (3) The energy used and the total amount of material compaction for the whole welding process indicate whether the weld formation at the interface is completed.
- (4) The relationships between weld attributes and several signal features such as total energy (E_{total}), midpoint energy (E_{mid}), total material compaction (D_{total}), and midpoint material compaction (D_{mid}) provide additional physical understanding of the impact of process conditions on the weld quality. They can be used to establish criteria for weld quality monitoring.

Acknowledgment:

Mr. **J MURALI NAIK, M.Tech (Ph.D)** Avanthi Institute of Engineering and technology, Dept. of Mechanical Engineer, was gratefully acknowledged for guiding to Ultrasonic metal welding system and sensor signal acquisition test facility used in this international paper.

REFERENCE:

- [1] Kim, T. H., Yum, J., Hu, S. J., Spicer, J. P., and Abell, J. A., 2011, "Process Robustness of Single Lap Ultrasonic Welding of Thin, Dissimilar Materials," *CIRP Ann.*, 60(1), pp. 17–20.
- [2] Lee, S. S., Kim, T. H., Hu, S. J., Cai, W., and Abell, J. A., 2010, "Joining Technologies for Automotive Lithium-Ion Battery Manufacturing: A Review," *ASME Intl' Mnfg. Sci. and Eng. Conference*, Erie, PA, October 12–15, Vol. 1, pp. 541–549.
- [3] Lee, S. S., Kim, T. H., Hu, S. J., Cai, W., Abell, J. A., and Li, J., 2013, "Characterization of Joint Quality in Ultrasonic Welding of Battery Tabs," *ASME J. Manuf. Sci. Eng.*, 135(2), p. 021004.
- [4] Zhang, C., and Li, L., 2009, "A Coupled Thermal-Mechanical Analysis of Ultrasonic Bonding Mechanism," *Metall. Mater. Trans. B*, 40(2), pp. 196–207.
- [5] Kang, B., Cai, W., and Tan, C.-A., 2013, "Dynamic Response of Battery Tabs Under Ultrasonic Welding," *ASME J. Manuf. Sci. Eng.*, 135(5), p. 051013.
- [6] Lee, D., Kannatey-Asibu, E., and Cai, W., 2013, "Ultrasonic Welding Simulations for Multiple Layers of Lithium-Ion Battery Tabs," *ASME J. Manuf. Sci. Eng.*, 135(6), p. 061011.
- [7] Kong, C., Soar, R., and Dickens, P., 2003, "Characterisation of Aluminium Alloy 6061 for the Ultrasonic Consolidation Process," *Mater. Sci. Eng. A*, 363(1–2), pp. 99–106.
- [8] Kong, C., Soar, R., and Dickens, P. M., 2005, "A Model for Weld Strength in Ultrasonically Consolidated Components," *Proc. Inst. Mech. Eng., Part C*, 219(1), pp. 83–91.
- [9] Siddiq, A., and Ghassemieh, E., 2009, "Theoretical and Fe Analysis of Ultrasonic Welding of Aluminum Alloy 3003," *ASME J. Manuf. Sci. Eng.*, 131(4), p. 041007.
- [10] Gunduz, I. E., Ando, T., Shattuck, E., Wong, P. Y., and Doumanidis, C. C., 2005, "Enhanced Diffusion and Phase Transformations During Ultrasonic Welding of Zinc and Aluminum," *Scr. Mater.*, 52(9), pp. 939–943.
- [11] Li, J., Han, L., and Zhong, J., 2008, "Short Circuit Diffusion of Ultrasonic Bonding Interfaces in Microelectronic Packaging," *Surf. Interface Anal.*, 40(5), pp. 953–957.
- [12] Annoni, M., and Carboni, M., 2011, "Ultrasonic Metal Welding of Aa 6022-T4 Lap Joints: Part I-Technological Characterisation and Static Mechanical Behaviour," *Sci. Technol.*

- Weld. Joining, 16(2), pp. 107–115.
- [13] Chu, Y., Hu, S., Hou, W., Wang, P., and Marin, S., 2004, “Signature Analysis for Quality Monitoring in Short-Circuit GMAW,” *Weld. J.*, 83(12), pp. 336–343.
- [14] Hu, S., Hou, W., Du, H., Wang, P.-C., and Menassa, R. J., 2011, “Method for Controlling the Consistency of an Arc Welding Process by Monitoring Welding Voltage to Determine Weld Droplet Detachment,” U.S. Patent No. US8063340 B2.
- [15] Shao, C., Paynabar, K., Kim, T. H., Jin, J., Hu, S. J., Spicer, J. P., Wang, H., and Abell, J. A., 2013, “Feature Selection for Manufacturing Process Monitoring Using Cross-Validation,” *J. Manuf. Syst.*, 32(4), pp. 550–555.
- [16] Ling, S.-F., Wan, L.-X., Wong, Y.-R., and Li, D.-N., 2010, “Input Electrical Impedance as Quality Monitoring Signature for Characterizing Resistance Spot Welding,” *NDT & E Int.*, 43(3), pp. 200–205.
- [17] Li, W., Hu, S. J., and Ni, J., 2000, “On-Line Quality Estimation in Resistance Spot Welding,” *ASME J. Manuf. Sci. Eng.*, 122(3), pp. 511–512.
- [18] Tseng, K. H., and Chuang, K. J., 2012, “Monitoring Nugget Size of Micro Resistance Spot Welding (Micro Rsw) Using Electrode Displacement-Time Curve,” *Adv. Mater. Res.*, 463, pp. 107–111.
- [19] Park, Y. W., and Kim, D., 2012, “Optimization of Laser Welding Parameters in Aluminum Alloy Welding and Development of Quality Monitoring System for Light Weight Vehicle,” *Mater. Sci. Forum*, 706–709, pp. 2998–3003.
- [20] Sun, A., Kannatey-Asibu, E., and Gartner, M., 1999, “Sensor Systems for Real-Time Monitoring of Laser Weld Quality,” *J. Laser Appl.*, 11(4), pp. 153–168. Wu, C., Gao, J., and Hu, J., 2007, “Real-Time Sensing and Monitoring in Robotic Gas Metal Arc Welding,” *Meas. Sci. Technol.*, 18(1), pp. 303–310.
- [21] Or, S., Chan, H., Lo, V., and Yuen, C., 1998, “Ultrasonic Wire-Bond Quality Monitoring Using Piezoelectric Sensor,” *Sens. Actuators A*, 65(1), pp. 69–75.
- [22] Zhao, J., Li, H., Choi, H., Cai, W., Abell, J. A., and Li, X., 2013, “Insertable Thin Film Thermocouples for in Situ Transient Temperature Monitoring in Ultrasonic Metal Welding of Battery Tabs,” *SME J. Manuf. Process.*, 15(1), pp. 136–140.
- [23] Li, H., Choi, H., Ma, C., Zhao, J., Jiang, H., Cai, W., Abell, J. A., and Li, X., 2013, “Transient Temperature and Heat Flux Measurement in Ultrasonic Join-ing of Battery Tabs Using Thin-Film Microsensors,” *ASME J. Manuf. Sci. Eng.*, 135(5), p. 051015.
- [24] Jia, S., Hong, E., Katz, R., Lev, L. C., Smyth, S., and Abell, J., 2012, “Nondestructive Testing of Ultrasonic Welding Joints Using Shearography Technique,” *ASME J. Manuf. Sci. Eng.*, 134(3), p. 034502.
- [25] Gao, Y., and Doumanidis, C., 2002, “Mechanical Analysis of Ultrasonic Bonding for Rapid Prototyping,” *ASME J. Manuf. Sci. Eng.*, 124(2), pp. 426–434.
- [26] Bakavos, D., and Prangnell, P. B., 2010, “Mechanisms of Joint and Microstructure Formation in High Power Ultrasonic Spot Welding 6111 Aluminium Auto-motive Sheet,” *Mater. Sci. Eng.: A*, 527(23), pp. 6320–6334.
- [27] Patel, V. K., Bhole, S. D., and Chen, D. L., 2011, “Influence of Ultrasonic Spot Welding on Microstructure in a Magnesium Alloy,” *Scr. Mater.*, 65(10), pp. 911–914.
- [28] Prangnell, P., Haddadi, F., and Chen, Y., 2011, “Ultrasonic Spot Welding of Aluminium to Steel for Automotive Applications: Microstructure and Opti-misation,” *Mater. Sci. Technol.*, 27(3), pp. 617–624.
- [29] Lee, S. S., Kim, T. H., Cai, W. W., and Abell, J. A., 2014, “Parasitic Vibration Attenuation in Ultrasonic Welding of Battery Tabs,” *Int. J. Adv. Manuf. Tech-nol.*, 71(1–4), pp. 181–195.